Nuclear Instruments and Methods in Physics Research B 318 (2014) 15–18

Contents lists available at ScienceDirect

Nuclear Instruments and Methods in Physics Research B

journal homepage: www.elsevier.com/locate/nimb

Chemical effects correlated to nitrogen content of iron nitride films observed in the Fe L-shell X-rays induced by 5-keV electrons

R. Hinrichs [a,*], A.P.L. Bertol [b], S.D. Jacobsen [c], G. Castellano [d,e], M.A.Z. Vasconcellos [b]

[a] Instituto de Geociências, Universidade Federal do Rio Grande do Sul, Porto Alegre, RS, Brazil
[b] Instituto de Física, UFRGS, Porto Alegre, RS, Brazil
[c] Pós-graduação em Ciência dos Materiais, UFRGS, Porto Alegre, RS, Brazil
[d] Facultad de Matemática, Astronomía y Física, Universidad Nacional de Córdoba, Argentina
[e] Instituto Enrique Gaviola, CONICET, Argentina

ARTICLE INFO

Article history:
Received 16 March 2013
Received in revised form 6 May 2013
Accepted 27 May 2013
Available online 22 July 2013

Keywords:
Chemical shift
Chemical effect
WDS
Iron nitride
Fe L-shell X-rays

ABSTRACT

Iron nitride thin films, produced by reactive magnetron sputtering, were characterized with grazing incidence X-ray diffraction, X-ray reflectometry, Rutherford backscattering spectrometry (RBS) and conversion electron Mössbauer spectroscopy. Their characteristic L-X-rays spectra, obtained with an electron microprobe analyzer equipped with a wavelength dispersive spectrometer, were compared to the spectrum of an iron standard. The spectra from the nitrides presented several chemical effects: change in the relative peak areas and shifts of the positions of the $L\alpha_{1,2}$ and the $L\beta_1$ peaks (chemical shift). The change in relative peak areas, namely the ratio between the $L\beta_1$ and the $L\alpha_{1,2}$ peaks, correlated well with the nitrogen content measured with RBS.

1. Introduction

Iron nitride phases have been studied for a long time, due to their application in magnetic recording and because of their wear reducing properties when used as protective surface coatings. Iron nitrides can be obtained by various methods. It has been shown that reactive magnetron sputtering can produce phases encompassing the whole composition range in the phase diagram, even disclosing new phases and structures [1,2].

When nitrogen is a next neighbor to the iron atom, it influences the energy levels and the occupation of the outer electron shells of the iron atoms, reflecting on the X-rays emitted after core ionizations due to transitions that involve the valence electrons.

Chemical effects on the characteristic X-rays were perceived quite early [3–5], and the discovery and interpretation of the shifts in the X-ray spectra since the early 1920s were reviewed by Lindgren [6]. In X-ray spectroscopy, mainly the change in the $K\alpha/K\beta$ ratio of the characteristic X-rays of transition metals are reported [7–15]. The L-shell X-rays are affected as well, but have been less analyzed [16–19], as well as the satellite lines [20,21], and the absorption edges [22].

Many efforts have been made to distinguish the oxidation state of iron in minerals using the chemical effect [23], or the X-ray absorption near edge structure (XANES) [24], but only a few studies were related to other ligands of the iron atom than oxygen [3,4,9,13,15].

The electronic shells of free iron atoms are filled until [Ar] $3d^{5+1-}$ $4s^{1+1-}$ [25], while ideally Fe^{3+} corresponds to [Ar] $3d^{5+}$ and Fe^{2+} to [Ar] $3d^{5+1-}$. In iron metal, however, the mean density of states becomes [Ar] $3d^{4.8+,2.6-}$ $4s^{0.3+,0.3-}$ [25]. Many stoichiometric and non-stoichiometric nitrides are possible, e.g. ε-$Fe_{2-3}N$, γ'-Fe_4N, and $\gamma''/\ \gamma'''$FeN. Nagakura, while studying iron nitrides, determined the electronic occupation of the shells, e.g. of $\gamma'Fe_4N$ as Fe $(Fe^{+1/3})_3N^{-1}$ [26], using the superstructure intensities in electron diffraction patterns. With nuclear reactionanalysis the analysis of nitrogen content is restricted to films with thickness below 200 nm [27]. With EPMA, as in this work, the chemical effect on the iron L-lines can be used to estimate the nitrogen content up to film thicknesses of 500 nm, using 5 keV electrons and considering their range and ability to ionize the iron-L-shell [28].

In this work we report on the findings that several chemical effects on the Fe-L X-ray emissions relate to the nitrogen content in ~20 nm iron nitride layers deposited by reactive magnetron sputtering, using atmospheres with different ratios of N_2/Ar.

* Corresponding author. Tel.: +55 51 33087144.
E-mail address: ruth.hinrichs@ufrgs.br (R. Hinrichs).

0168-583X/$ - see front matter © 2013 Elsevier B.V. All rights reserved.
http://dx.doi.org/10.1016/j.nimb.2013.05.101

2. Materials and methods

2.1. Sample preparation

Iron nitride films were deposited on silicon wafers as well as on vitreous carbon planchets (Ted Pella) using reactive magnetron sputtering in a ultra-high vacuum equipment (AJA International model ATC, ORION 8 UHV): one film (Fe_xN_yh) in a high N_2 atmosphere (80 vol.% N_2: 20 vol.% Ar) and the other (Fe_xN_yl) in a low N_2 content atmosphere (40 vol.% N_2: 60 vol.% Ar). The gas flows were controlled by two independent mass-flow controllers and adjusted to a total of 25 sccm (standard cubic centimeter). The deposition rate was kept at 2 nm/min, and deposition time was 10 min for both films. The deposition occurred at room temperature without further annealing. The characterizations were performed either on the films on top of the silicon wafer or on the carbon planchets.

2.2. Sample characterization

The samples were analyzed with grazing incidence X-ray diffraction (GIXRD) in Seeman Bohlin geometry using 0.5° incidence angle, in the 2θ range from 20° to 70° (Shimadzu XRD6000, with Cu-tube and thin film attachment). The diffractograms were interpreted with the cards from the powder diffraction file (PDF-2) and the grain size determined using the Scherrer formula, when peaks were observable.

The X-ray reflectivity (XRR) was measured in the same XRD6000 equipment in Bragg–Brentano geometry, in the 2θ range from 0.5° to 5°. The Xpert reflectivity software (Panalytical) was used for thickness determination.

The thickness and composition was analyzed with Rutherford backscattering spectrometry (RBS) in a 3 MV Tandetron (High Voltage Engineering), using alpha particles accelerated to 1 MeV. The code SIMNRA [29] was used to fit the experimental results and to obtain the mass thickness and composition.

Conversion electron Mössbauer spectroscopy (CEMS) was performed in backscattering geometry (Wissel spectrometer) using a ^{57}Co in Rh source to excite the ^{57}Fe atoms in the sample. The hyperfine parameters (magnetic field, isomer shift, and quadrupole splitting) were adjusted using the software Wfitting.

2.3. L-X-ray spectra

The Fe-L-lines from the two films and a bulk iron standard were acquired using an electron probe micro-analyzer (EPMA JEOL JXA 8230) equipped with a wavelength dispersive spectrometer (WDS) containing a TAP (1011) analyzing crystal ($2d$ = 25.76 Å). The beam energy was kept at 5 keV. The spectra were processed subtracting the linear background and fitting the lines with 5 Lorentzian peaks (Origin6®).

3. Characterization

3.1. Grazing incidence X-ray diffraction (GIXRD)

The diffractograms showed that the films had low crystallinity, with broad peaks. While the sample Fe_xN_yh seemed amorphous, it was possible to estimate the grain size of sample Fe_xN_yl to be ~7 nm. The possible phases in this sample were identified as FeN (PDF number 50-1087), Fe_2N (PDF number 76-0090), $Fe_{2-3}N$ (PDF number 86-1025), and contamination with magnetite (PDF number 76-1849).

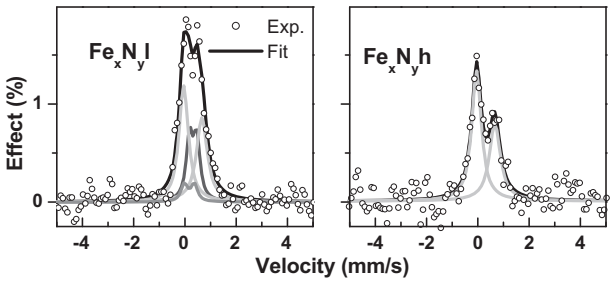

Fig. 1. CEMS of the nitrided samples. Open symbols are the experimental data, black solid lines are the sum of the partial spectra (see Section 3.4).

3.2. X-ray reflectivity (XRR)

The thicknesses of the nitrided layers were estimated with the aid of the X-ray reflectograms. The Fourier transforms of the XRR patterns indicated a strong peak at 18 nm for sample Fe_xN_yh and 17 nm for Fe_xN_yl. The uncertainty in the thickness value was estimated from the width of the Fourier transform. Each oscillation was analyzed individually as well, and the mean thickness and standard deviation were consistent with the values obtained in the Fourier analysis.

3.3. Rutherford backscattering spectrometry (RBS)

RBS measurements showed the presence of iron, nitrogen and oxygen on the carbon substrate. Fe_xN_yl showed a small contamination with sulfur, due to a handling mishap. Simulations with the software SIMNRA indicated a mass thickness of $163{\cdot}10^{15}$ at/cm^2 for Fe_xN_yh and of $187{\cdot}10^{15}$ at/cm^2 for Fe_xN_yl. The N/Fe ratio was 0.88 for Fe_xN_yh and 0.56 for Fe_xN_yl, however the uncertainty associated with the nitrogen analyses was around 30%.

3.4. Conversion electron Mössbauer spectroscopy (CEMS)

The CEMS spectra for the two iron nitride thin films are displayed in Fig. 1. Both CEMS patterns presented an asymmetric double peak, representing nonmagnetic phases. Fe_xN_yh was fitted with the two components of γ″/γ″FeN [30]: (i) a singlet with an isomer shift of 0.06 mm/s and area fraction of 59%, associated to Fe in tetrahedral N coordination; (ii) a singlet with isomer shift of 0.55 mm/s and area fraction of 41%, attributed to the contribution of defects and vacancies in the same structure. In the Fe_xN_yl spectrum the asymmetry was lower and the spectrum did not fit with the γ″/γ″FeN singlets alone, but needed the addition of thetwo doublets of the ε-$Fe_{2.1}$N [31]. The CEMS spectra were able to discriminate the nitride phases, even in the Fe_xN_yh sample, that appeared amorphous in GIXRD. The difference between the crystallinity of the two films, however, was reflected as well in the broader peaks of the CEMS spectra of sample Fe_xN_yh. In Fig. 1 the γ″/γ″FeN singlets are shown in light grey and the ε-$Fe_{2.1}$N doublets in dark grey.

4. Results and discussion

The bonding to a ligand causes an effect on those L-shell X-rays of the iron atom that are produced when the hole in the L-shell is supplied by electrons that participate in the bonding, as are the 3d or 4s electrons. To remind the reader of the structure of the energy levels and the possible electronic transitions, a diagram with the

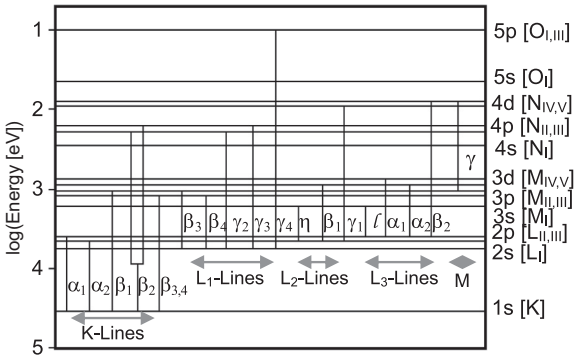

Fig. 2. Energy levels and line nomenclature (adapted from [32]).

nomenclature of the lines is displayed in Fig. 2 [32]. It can be seen that e.g. the Ll and Lη X-rays are due to transitions from electrons of the 3s level, while the $L\beta_{3,4}$ X-ray comes from a transition of electrons from the 3p level, that do not participate in chemical bonding. No transitions are allowed from the 4s level to an L-shell hole, therefore only the 3d electrons, producing $L\alpha_{1,2}$ and $L\beta_1$ X-rays are affected.

The WDS spectra of a bulk iron standard and of the two iron nitride films are shown in Fig. 3. The observed Fe L-lines correspond to the transitions $L_{III}M_{IV,V}$ ($L\alpha_{1,2}$), $L_{II}M_{IV}$ ($L\beta_1$), $L_{III}M_I$ (Ll), $L_{II}M_I$ (Lη), and $L_IM_{II,III}$ ($L\beta_{3,4}$). It is apparent, that the position of the Ll-line is

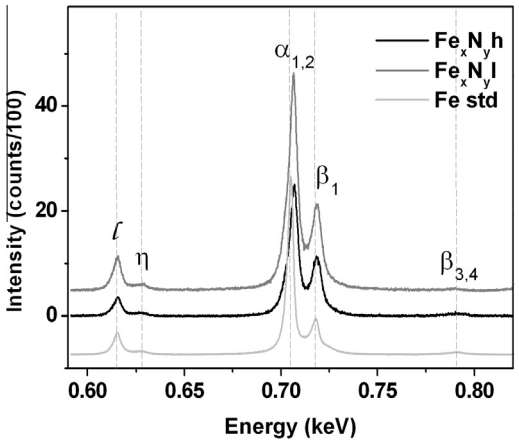

Fig. 3. EPMA–WDS spectra of the nitrided samples and a bulk iron standard.

Table 1
Peak parameters obtained from the Lorentzian least square fit of the WDS spectra. Bracketed numbers indicate the uncertainty of the last digit.

L-lines		Fe_xN_yh	Fe_xN_yl	Std
1	Position in eV	615.41(4)	615.30(4)	615.24(4)
	Width	4.6(1)	4.6(1)	4.4(1)
	% of $L\alpha_{1,2}$ area	12.2(2)	13.0(2)	14.7(2)
η	Position above L_l	12.0(3)	12.4(3)	12.1(4)
	Width	4.3(9)	4.6(8)	5.6(1)
	% of $L\alpha_{1,2}$ area	1.6(2)	1.8(2)	2.3(3)
$\alpha_{1,2}$	Position above L_l	91.21(7)	90.98(6)	89.74(4)
	Width	5.53(2)	5.53(2)	3.57(1)
	% of $L\alpha_{1,2}$ area	100(3)	100(3)	100.0(2)
β_1	Position above L_l	103.29(2)	103.37(2)	102.62(3)
	Width	5.36(5)	5.40(5)	5.45(9)
	% of $L\alpha_{1,2}$ area	42.4(2)	37.19(2)	27.4(3)
$\beta_{3,4}$	Position above L_l	174.6(3)	174.6*	175.3(6)
	Width	5*	5*	8(2)
	% of $L\alpha_{1,2}$ area	1.8(2)	0.1(1)	2.4(3)

* The peak intensity was so low, that the position and/or width of the peak had to be fixed in the fitting procedure, otherwise the fit diverged.

not altered, while $L\alpha_{1,2}$ and $L\beta_1$ shift to higher energies. Lη and $L\beta_{3,4}$ X-ray are of low intensity, and their modifications are not discernible by simple inspection of the spectra.

The spectra were fitted with 5 Lorentzian curves (Origin6®) and the obtained fit parameters (positions, widths, and areas of the peaks) and uncertainties are presented in Table 1. The fit parameters revealed that the peak positions of the Ll X-rays was stable within 1 eV. Peak width was stable too, peak area varied between 12% and 15% of the main $L\alpha_{1,2}$ peak. The Lη peak had a low intensity (relative area between 1.6% and 2.3%) and the peak position was stable within 0.4 eV. The $L\alpha_{1,2}$ peak after nitriding assumed a position of 91.1(0.1) eV above the Ll line, while in the iron standard the difference was 89.7 eV. The width of the $L\alpha_{1,2}$ peak increased to 5.4 eV, compared to 3.6 eV in the standard. The $L\beta_1$ peak position changed less than the $L\alpha_{1,2}$. The relative area showed the most significant change with increasing N content – it changed to 42.4% of the $L\alpha_{1,2}$ peak in the film with maximum nitrogen content, and to 37.2% in the intermediate one, compared to 27.4% in the iron standard.

When the parameters of the three most preeminent peaks were compared as bar plots (Fig. 4), it became apparent that some chemical effects, as e.g. the relative intensity of the lines, occurred due to the nitriding, and increasingly so as the nitrogen content was higher.

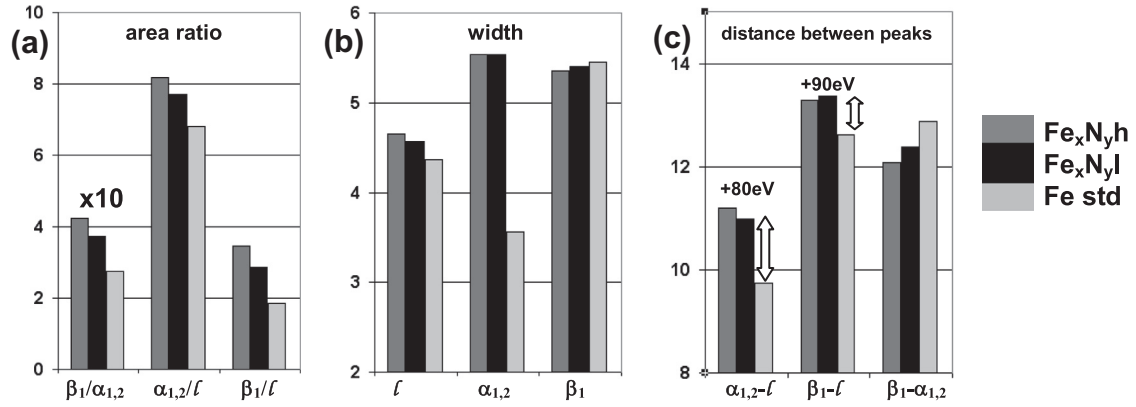

Fig. 4. Comparison of (a) the peak area ratios, (b) the peak widths, and (c) the distance distances between indicated peaks in the nitrided samples and the Fe standard. The chemical shifts of the $L\alpha_{1,2}$ and $L\beta_1$ peaks are indicated with block arrows in (c).

Sakuna [33] showed that the number of electrons in the Fe 3d band increases with increasing nitrogen content (Table 1 in reference [33]). This effect can be seen in our spectra as an increase of the area of transitions that involve the 3d levels ($L\alpha_{1,2}$ and $L\beta_1$) when compared to the area of a transition that does not, e.g. Ll (3s to $2p_{1/2}$)in Fig. 4a.

Only the $L\alpha_{1,2}$ line width (Fig. 4b) showed a significant broadening (from 3.7 eV to 5.5 eV), effect that can be due to changes in the relative population of the $Fe3d_{1/2}$ and Fe $3d_{3/2}$ levels, however the strong overlap of the $L\alpha_1$ and $L\alpha_2$ lines rendered it difficult to ascertain this hypothesis.

The peak shift (block arrows in Fig. 4c) is indicated relative to the position of the Ll line in the spectrum. It can be seen that the nitriding induced a chemical shift, however not so clearly correlated with the nitrogen content as the peak area ratios that are highest for the highest nitrogen content.

5. Conclusions

We showed that the there are chemical effects on the iron Lshell due to the bonding to different amounts of nitrogen in thin iron nitride films produced by reactive magnetron sputtering. The area ratio between the $L\alpha_{1,2}$ peak and the Ll-peak showed the most significant change with increasing N content. Considering that the nitrogen content observed in the RBS measurements is compatible with the phases seen in CEMS, the observed effects can be used as an additional phase recognition method. This technique allows the analysis of thicker nitride films, as those used in wear coatings obtained by conventional glow discharge plasma nitriding.

Acknowledgements

The authors thank the Laboratório de Conformação Nanométrica, IF-UFRGS for film preparation, and the Laboratório de Implantação Iônica, IF-UFRGS for RBS measurements. They also acknowledge financial support from the Brazilian funding agencies CAPES, CNPq, and FAPERGS and from the Argentinean SPU/Ministerio de Educación.

References

[1] E. Bradley Easton, T.H. Buhrmester, J.R. Dahn, Thin Solid Films 493 (2005) 60–66.
[2] X. Wang, W.T. Zheng, H.W. Tian, S.S. Yu, W. Xu, S.H. Meng, X.D. He, J.C. Han, C.Q. Sun, B.K. Tay, Appl. Surf. Sci. 220 (2003) 30–39.
[3] J. Blomquist, B. Roos, M. Sundbom, Chem. Phys. Lett. 9 (2) (1971) 160–162.
[4] L.Y. Johansson, R. Larsson, J. Blomquist, C. Cederström, S. Grapengiesser, U. Helgeson, L.C. Moberg, M. Sundbom, Chem. Phys. Lett. 24 (4) (1974) 508–513.
[5] L.Y. Johansson, J. Blomquist, Chem. Phys. Lett. 34 (1) (1975) 115–118.
[6] I. Lindgren, J. Electron Spectrosc, Relat. Phenom. 137–140 (2004) 59–71.
[7] T. Mukoyama, H. Kaji, K. Yoshihara, Phys. Lett. A 118 (1) (1986) 44–46.
[8] O. Sogut, S. Seven, E. Baydas, E. Büyükkasap, A. Küçükönder, Spectrochim. Acta B 56 (8) (2001) 1367–1374.
[9] O. Sogut, E. Büyükkasap, H. Erdoğan, Radiat. Phys. Chem. 64 (5–6) (2002) 343–348.
[10] S. Fazinić, M. Jakšić, L. Mandić, J. Dobrinić, Phys. Rev. A 74 (062501) (2006) 1–12.
[11] A. Gürol, Appl. Radiat. Isot. 66 (3) (2008) 372–376.
[12] L. Mandić, S. Fazinić, M. Jakšić, Phys. Rev. A 80 (042519) (2009) 1–10.
[13] E. Baydaş, E. Öz, J. Electron Spectrosc. Relat. Phenom. 185 (1–2) (2012) 27–31.
[14] S. Fazinić, L. Mandić, M. Kavčič, I. Božičević, J. Anal. At. Spectrom. 26 (2011) 2467–2476.
[15] K. Kaur, R. Mittal, Radiat. Phys. Chem. 83 (2013) 28–33.
[16] E. Baydaş, Ö. Söğüt, Y. Şahin, E. Büyükkasap, Radiat. Phys. Chem. 54 (3) (1999) 217–221.
[17] J. Iihara, C. Izawa, T. Omori, K. Yoshihara, Nucl. Instr. Meth. Phys. Res. Sect. A 299 (1–3) (1990) 394–398.
[18] J. Iihara, T. Omori, K. Yoshihara, K. Ishii, Nucl. Instr. Meth. Phys. Res. Sect. B 75 (1–4) (1993) 32–34.
[19] J. Kawai, K. Nakajima, Y. Gohshi, Spectrochim. Acta Part B 48 (10) (1993) 1281–1290.
[20] J. Kawai, C. Satoko, Y. Gohshi, Spectrochim. Acta Part B 42 (10) (1987) 1125–1137.
[21] M. Torres-Deluigi, J.A. Riveros, Chem. Phys. 325 (2006) 472–476.
[22] K.S. Srivastava, V. Kumar, J. Phys. Chem. Solids 42 (4) (1981) 275–280.
[23] H.E. Höfer, G.P. Brey, Am. Mineral. 92 (2007) 873–885.
[24] A.J. Berry, G.M. Yaxley, A.B. Woodland, G.J. Foran, Chem. Geol. 278 (1–2) (2010) 31–37.
[25] J.C. Mallison, The Foundations of Magnetic Recording, Academic Press, SanDiego, 1993.
[26] S. Nagakura, J. Phys. Soc. Jpn. 25 (1968) 488–498.
[27] L. Rissanen, P. Schaaf, M. Neubauer, K.-P. Lieb, J. Keinonen, T. Sajavaara, Appl. Surf. Sci. 138–139 (1999) 261–265.
[28] K. Kanaya, S. Okayama, J. Appl. Phys. D 5 (1972) 43–58.
[29] M. Mayer, SIMNRA User Guide Technical Report IPP 9/113, Max Plank Institut für Plasmaphysik, Garching, Germany, 1997.
[30] M. Gupta, A. Tayal, A. Gupta, V.R. Reddy, M. Horisberger, J. Stahn, J. Alloys Comp. 509 (2011) 8283–8288.
[31] D.M. Borsa, D.O. Boema, Hyperfine Interact. 151 (152) (2003) 31–48.
[32] J.H. Wittke, http://www4.nau.edu/microanalysis/microprobe/Xray-NamingTransitions.html, (Acessed 03.15.2013).
[33] A. Sakuna, Self-consistent calculations for the electronic structures of iron nitrides, Fe3N, Fe4N and Fe16N2, J. Mag. Mag. Mat. 102 (1991) 127–134.